Supporting Information

Phosphorus-doped $Ti_3C_2T_x$ MXene nanosheets enabling ambient NH_3 synthesis with high current densities

Yuchuan Qi[a†], Xianghua Hou[a†], Ziying He[b]*, Fan He[a], Tianran Wei[b,c], Ge Meng[a]*, Huihui Hu[c], Qian Liu[d], Guangzhi Hu[e], and Xijun Liu[c]*

a Key Laboratory of Carbon Materials of Zhejiang Province, College of Chemistry and Materials Engineering, Wenzhou University, Wenzhou 325035, China. E-mail: mengge@wzu.edu.cn.

b Guangxi Vocational & Technical Institute of Industry, Nanning 530001 Guangxi, China. E-mail: 2021028852@gxgy.edu.cn.

c State Key Laboratory of Featured Metal Materials and Life-cycle Safety for Composite Structures, MOE Key Laboratory of New Processing Technology for Nonferrous Metals and Materials, School of Resources, Environment and Materials, Guangxi University, Nanning, 530004 Guangxi, China. E-mail: xjliu@gxu.edu.cn.

d Institute for Advanced Study, Chengdu University, Chengdu 610106, Sichuan, China.

e Institute for Ecological Research and Pollution Control of Plateau Lakes School of Ecology and Environmental Science, Yunnan University, Kunming 650504, China.

† These authors contributed equally to this work.

Experimental section

Chemicals

Lithium fluoride (LiF), and Ti_3AlC_2 powers were purchased from Macklin Reagent Company. Hydrochloric acid (HCl, 37.2%), potassium nitrate (KNO_3),and potassium sulfate anhydrous (K_2SO_4) were purchased from Aladdin Ltd (China). Nafion solution (5 wt%) were purchased from Alfa Aesar. Note that all the chemicals (analytical grade) were purchased from Aladdin and used directly without further purification here. Deionized water was purified through a Millipore system.

Synthesis of P-$Ti_3C_2T_x$ MXene nanosheets

2D $Ti_3C_2T_x$ MXene nanosheets were synthesized via a reported procedure according to our previous literature [1]. After that, the obtained $Ti_3C_2T_x$ was mixed with NaH_2PO_2 in two crucibles and the weight ratio of $Ti_3C_2T_x$ and NaH_2PO_2 was set to 1:2, 1:3, 1:5, and 1:7. After that, the residue was annealed in a tube at 500 °C for 3 h under an Ar atmosphere. The annealed sample was washed with 70 °C deionized water and ethanol to remove any residual chemicals, followed by drying in a vacuum oven. The reference $Ti_3C_2T_x$ sample was prepared using the same procedure but in the absence of NaH_2PO_2.

Material characterizations

The structural and micro-morphological features of these samples were taken from a JSM 6300F field emission scanning electron- microscope (SEM)

(JEOL) as well as a Tecnai G2 F30 transmission electron microscope (TEM) (FEI). At the same time, their crystal structure and phase composition were analyzed via an X-ray diffractometer (XRD) (PANalytical X'Pert Pro diffractometer) with Cu K_α radiation (λ = 1.5406 Å). Further, the chemical environment of the samples was recorded by the X-ray photoelectron spectrometer (XPS) from the Thermo Scientific K-Alpha (Shimadzu Kratos) with an Al (K_α) radiation probe (λ = 0.834 nm) and calibrated with C 1s of 284.8 eV.

NO_3RR tests

The electrochemical tests were performed in an electrolyte consisting of 0.5 M K_2SO_4 and 0.1 M KNO_3 by using an H-cell with a three-electrode configuration and separated by the proton exchange membrane (Nafion-117). The data was collected by the CHI 760E electrochemical workstation. To prepare the working electrode, 5 mg P-$Ti_3C_2T_x$ powder was homogeneously dispersed in a 1 mL mixture (50 μL 5 wt% Nafion and 950 μL 5 wt% EtOH) to obtain a catalyst ink, and then 30 μL ink was loaded onto carbon paper to get working electrode (0.15 mg cm^{-2}). The graphite rod and saturated Hg/Hg_2Cl_2 were employed as counter electrode and reference electrode, respectively. All applied potentials were converted to the reversible hydrogen electrode (RHE): E (*vs* RHE) = E (*vs* Hg/Hg_2Cl_2) + 0.244 + 0.0591 × pH. Quantification of NH_3 from NO_3RR was performed with a UV-Vis spectrometer (Shimadzu UV-2700).

Flow cell measurements

In the flow cell, the anodic and cathodic chambers were separated by a piece of proton exchange membrane (Nafion 211). A piece of commercial gas diffusion electrode (GDE, YLS-30T) was used to separate the cathodic chamber and NH_3 capture chamber. The side of the GDE loaded with catalyst was in contact with the cathode chamber, while the back side was in contact with the NH_3 capture chamber. A piece of GDE, Ni rod, and Hg/Hg_2Cl_2 electrode were used as working electrode, counter electrode, and reference electrode, respectively. During the NO_3RR test, the cathodic electrolyte (1 M K_2SO_4 + 0.5 M KNO_3) was continuously cycled through the cathode chamber with a rate of 60 mL min^{-1} under the pump drive. The 0.25 M H_2SO_4 solution was adopted to capture NH_3, and the flow rate was also set to 60 mL min^{-1}.

Determination of NH_3: Ammonia produced in the NO_3RR process was colored by the indophenol blue method and detected by the UV-Vis spectroscopy (IR Tracer-100, Shimadzu). Due to the high concentration of the product, all electrolytes after electrolysis were diluted 20 times before color development. After 1 hour of electrolysis, 2 mL of electrolyte was taken from the cathode cell, followed mixing with 2 mL colorant (containing salicylic acid, sodium citrate and sodium hydroxide), 1 mL of oxidant (0.05 M sodium hypochlorite), and 0.2 mL of catalyst solution (1 wt% sodium nitroferricyanide). Then, they were placed in the dark environment for 1 h, and the UV-Vis spectra were measured in the wavelength range from 550 to 800 nm. The absorption

intensity at 655 nm was substituted into the standard curve to quantify the ammonia yield.

Determination of NO_2^-: The method Griess Test was employed to detect the generated NO_2^- during electrolysis. For quantifying NO_2^-, a specific color reagent was prepared as follows: 0.4 g of p-aminobenzene sulfonamide and 0.02 g of N-(1-naphthyl) ethylenediamine dihydrochloride were dissolved in a mixture containing 5 mL of deionized water and 1 mL of phosphoric acid (ρ = 1.70 g/mL). To begin the detection process, a certain amount of electrolyte was extracted from the electrolytic cell and diluted to 5 mL to fit within the detection range. Next, 0.1 mL of the color reagent was added to the 5 mL of diluted electrolyte. The solution was left to stand for 20 min before testing, and its absorbance was measured using UV–Vis spectrophotometry at a wavelength of 540 nm.

Determination of N_2H_4: After 1 h of electrolysis, the electrolyte was diluted 16-fold to 2.5 mL, and 5.99 g of pp-dimethylamino benzaldehyde, 30 mL of hydrochloric acid, and 300 mL of ethanol were mixed into a uniform solution, which was used as a chromogen. Then, 2 mL of chromogen was added to 2 mL of electrolyte. After 20 minutes in dark, absorbance was performed at a wavelength from 420 to 500 nm. The absorbance at 455 nm is substituted into the standard curve to obtain the concentration of hydrazine.

Determination of H_2: The quantity of produced H_2 gas was assessed using Gas chromatography (7890A, Agilent) equipped with both a flame ionization

detector (FID) and a thermal conductivity detector (TCD). The thermal conductivity detector was utilized specifically for hydrogen quantification. All experiments were carried out within a sealed system.

DFT details

The P-$Ti_3C_2T_x$ model was constructed according to the report [1,2] under the density functional theory (DFT) in the Dmol^3 code. The lattice structure was set to periodic 2x2 unit cells, i.e., each structure has four layers of metal atoms including the fixed two layer bottom atom as well as other relaxed two layer atom for adsorbing objects. To analyze the Perdew-Burke-Emzerhof (PBE) exchange effect and related influence under the condition of generalized gradient approximation, the vacuum space was set to 15 Å. And, the Brillouin zone was sampled with 3 × 3 × 1, the real space global orbit truncation radius is set to 4.5 Å. Nuclear processes and atomic charges were analyzed by the effective core potential (ECP) and Hirshfeld method, respectively.

The free energy of atomic structure is determined as follows:

$$\triangle G = \triangle E + \triangle ZPVE + \int C_P dT - T \triangle S$$

where △E is the change of adsorption energy, △ZPVE is the difference of zero-point energy, and △S is the difference of entropy, C_p is the heat capacity, and T is the system temperature.

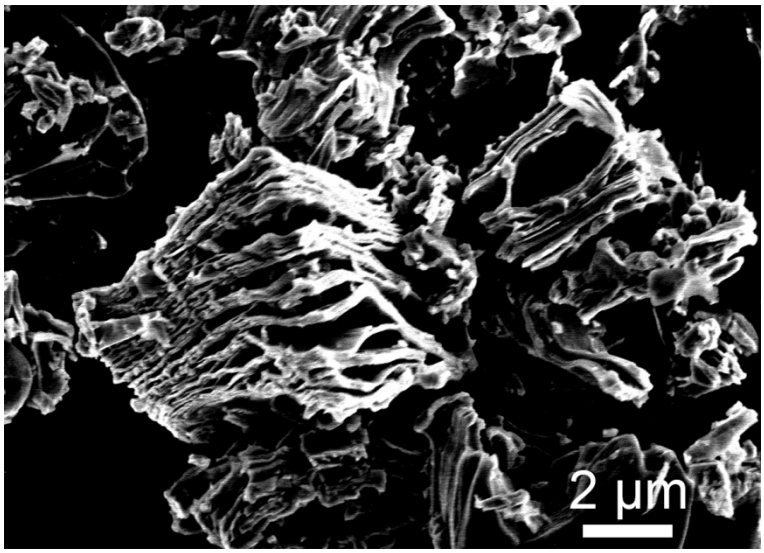

Figure S1. SEM image of the $Ti_3C_2T_x$ nanosheets.

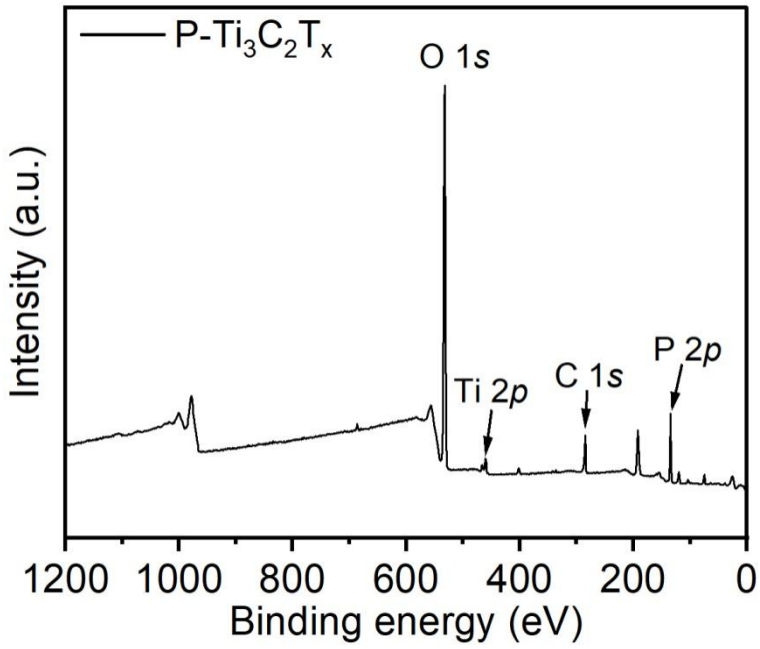

Figure S2. XPS survey spectrum for P-$Ti_3C_2T_x$.

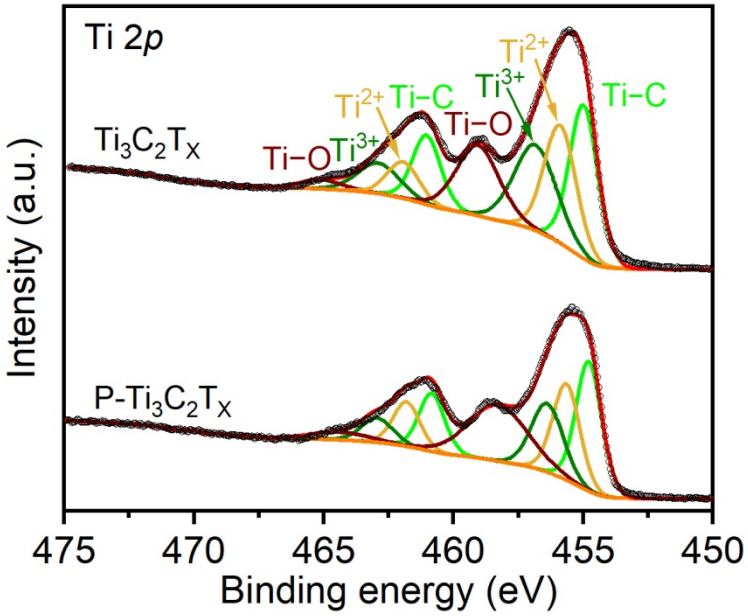

Figure S3. High-resolution Ti 2*p* XPS spectrum for P-$Ti_3C_2T_x$.

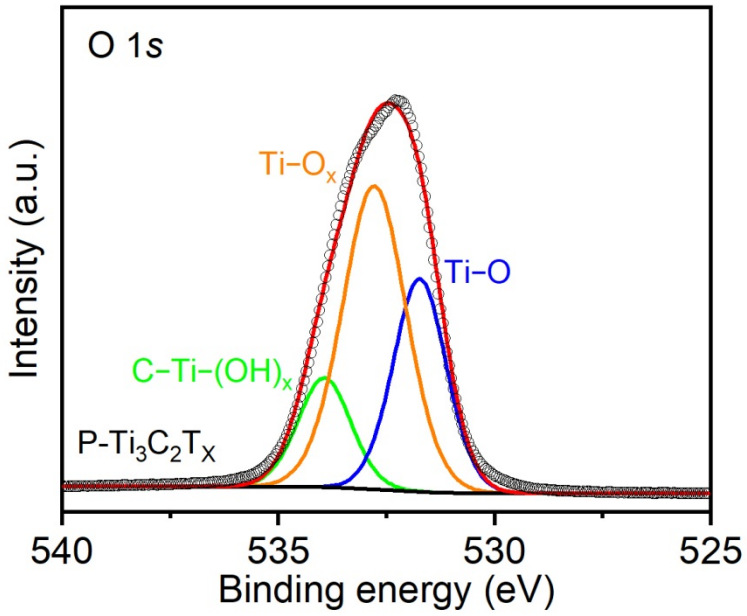

Figure S4. High-resolution O 1*s* XPS spectrum for P-$Ti_3C_2T_x$.

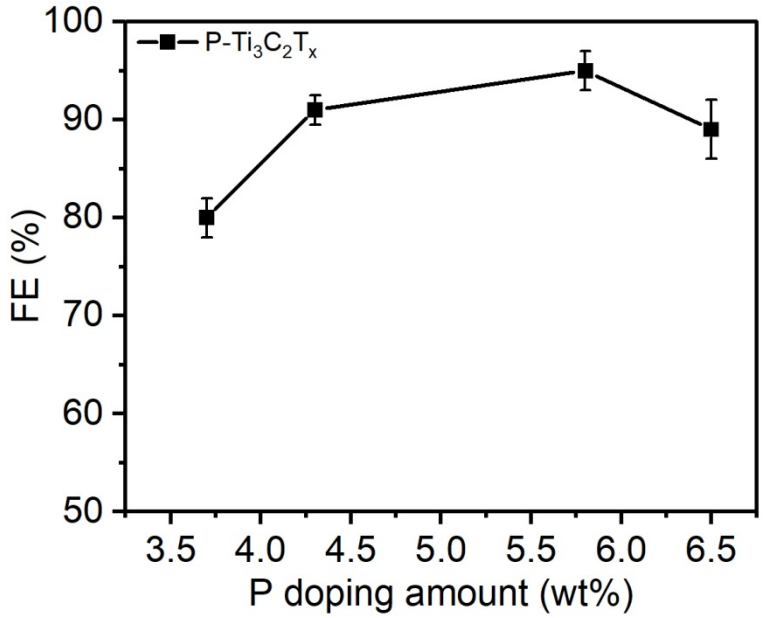

Figure S5. The NH_3 yield rates of the P-$Ti_3C_2T_x$ with different P doping amount performed at –1.2 V vs RHE.

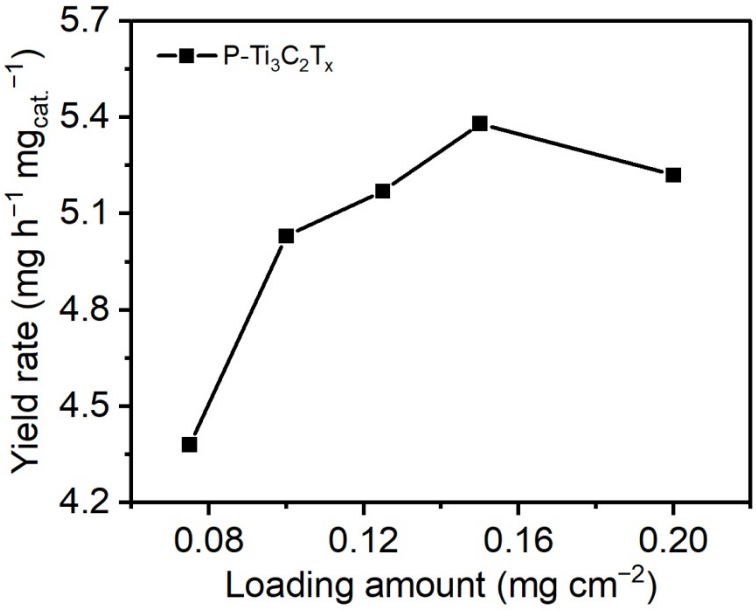

Figure S6. The NH_3 yield rates of the P-$Ti_3C_2T_x$ with different catalyst loading amount performed at –1.2 V vs RHE.

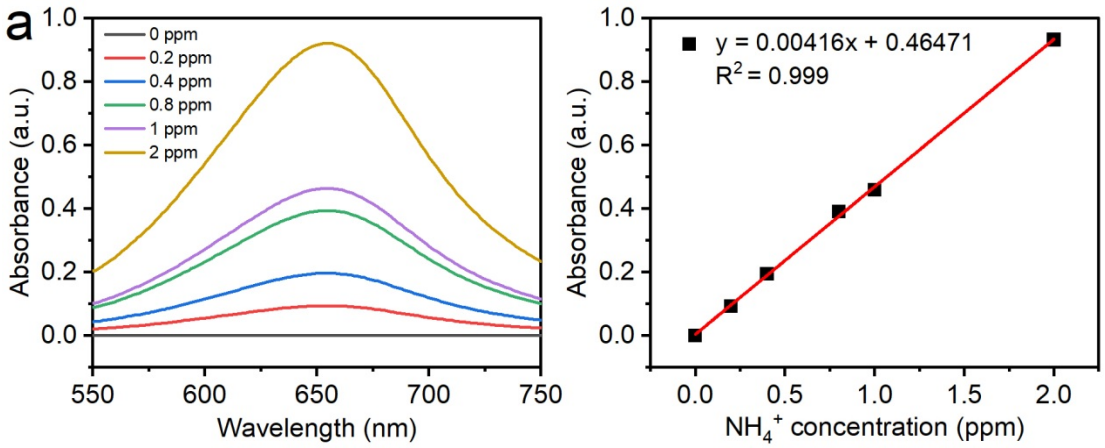

Figure S7. (a) UV-Vis absorption spectra of different concentrations of NH_3 stained with indophenol blue and (b) the corresponding calibration curve.

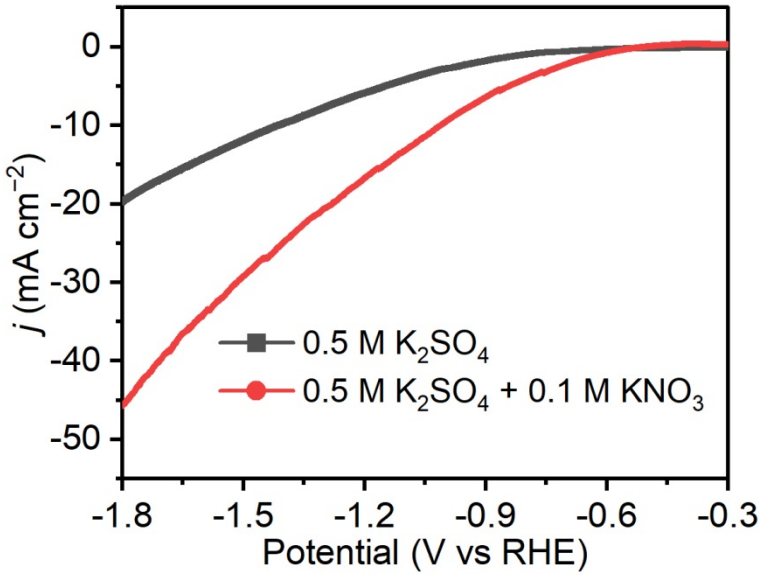

Figure S8. LSV curves of P-$Ti_3C_2T_x$ recorded in different electrolytes.

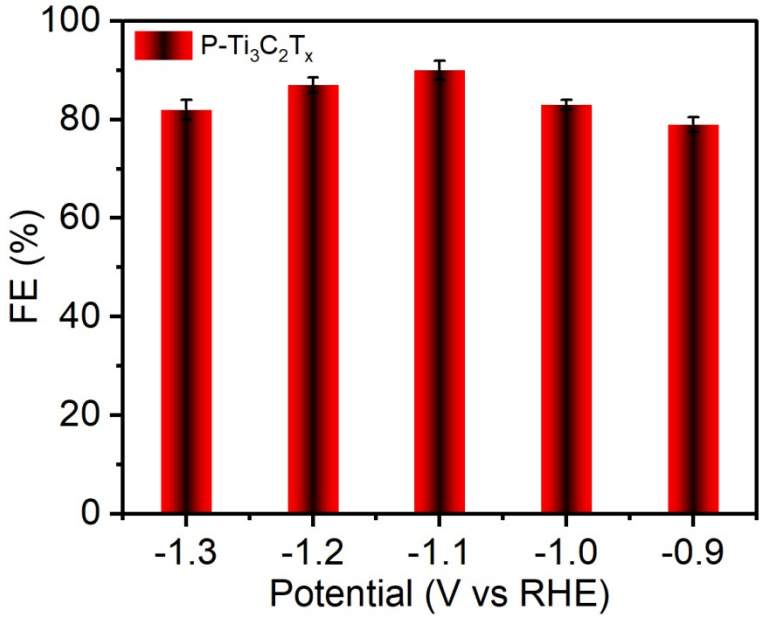

Figure S9. The obtained FEs and yield rates for P-$Ti_3C_2T_x$ in a electrolyte with 0.5 M K_2SO_4 + 0.05 M KNO_3.

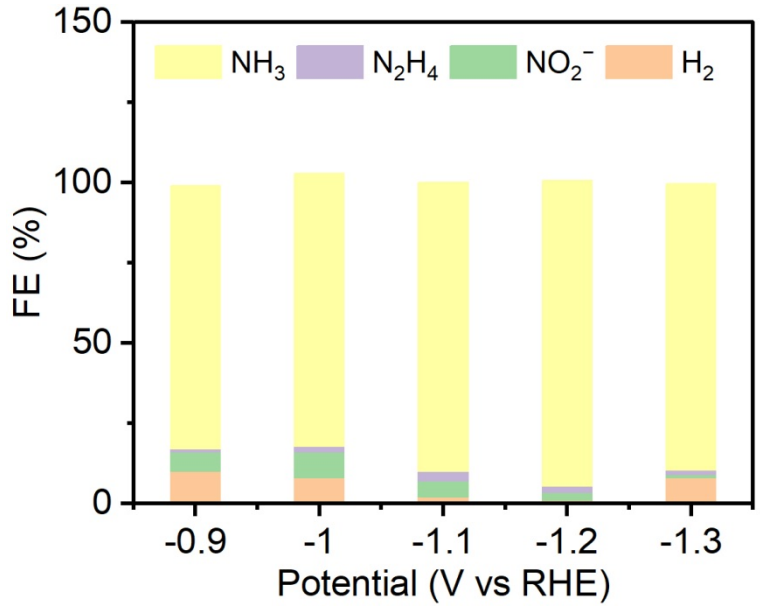

Figure S10. The FEs for the by-products of P-$Ti_3C_2T_x$.

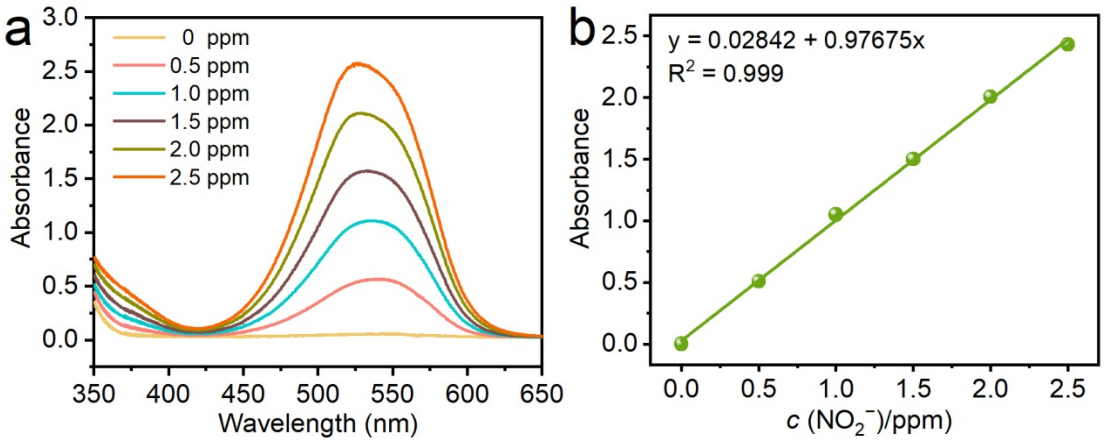

Figure S11. (a) UV-Vis absorption spectra of various concentrations of NO_2^- and (b) the corresponding calibration curve.

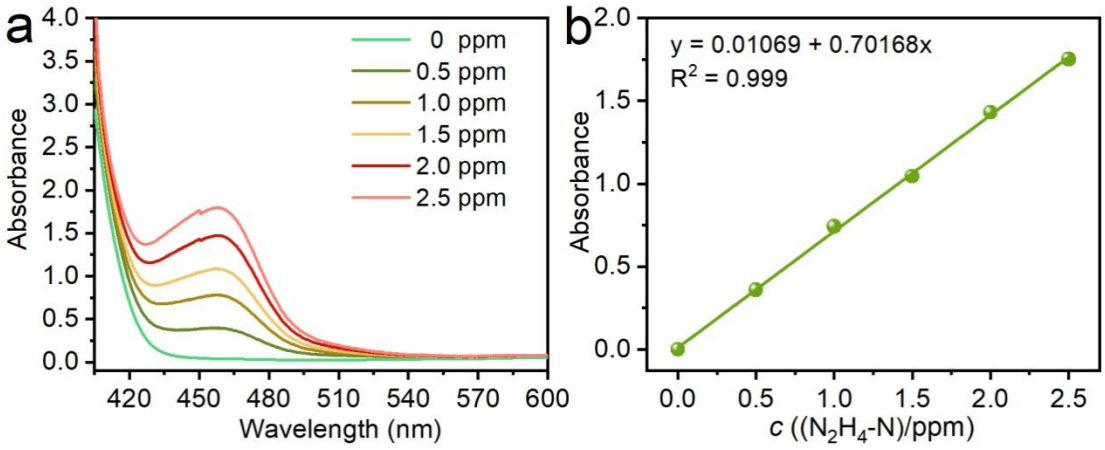

Figure S12. (a) UV-Vis absorption spectra of various concentrations of N_2H_4 and (b) the corresponding calibration curve.

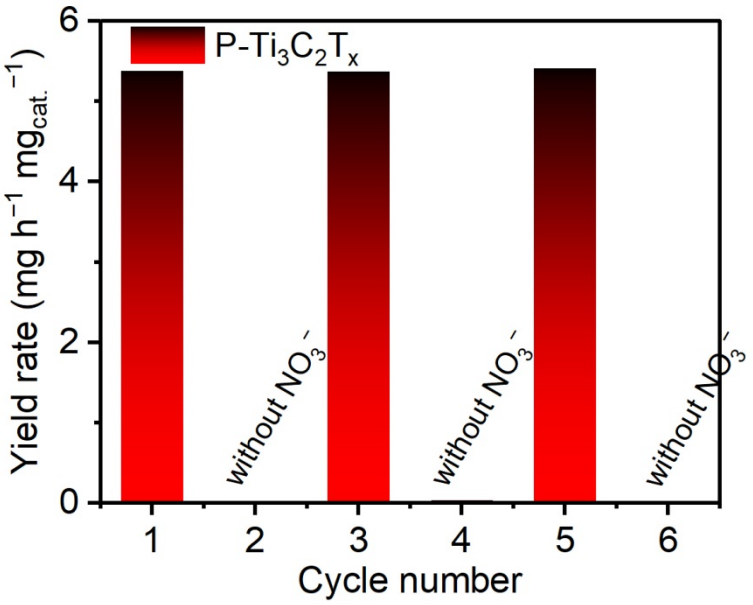

Figure S13. NO_3RR performance of P-$Ti_3C_2T_x$ after the alternating cycle measurement.

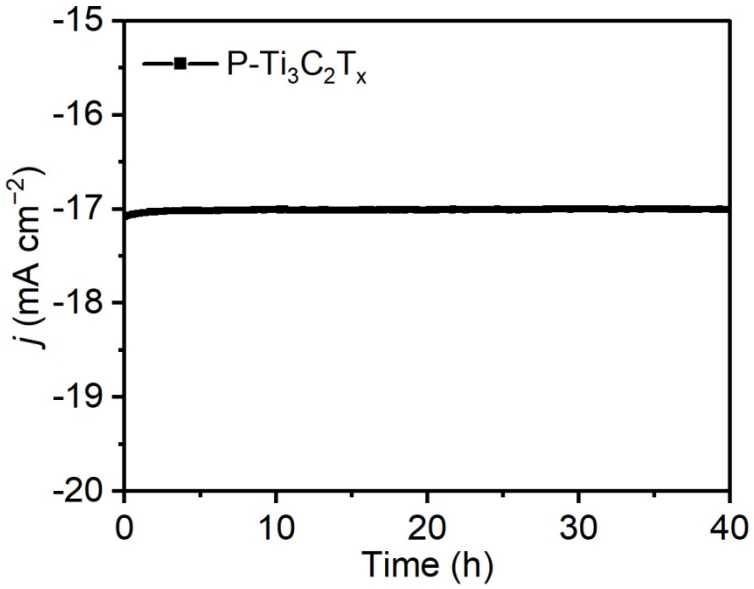

Figure S14. Long-term electrolysis at –1.2 V vs RHE over 40 h.

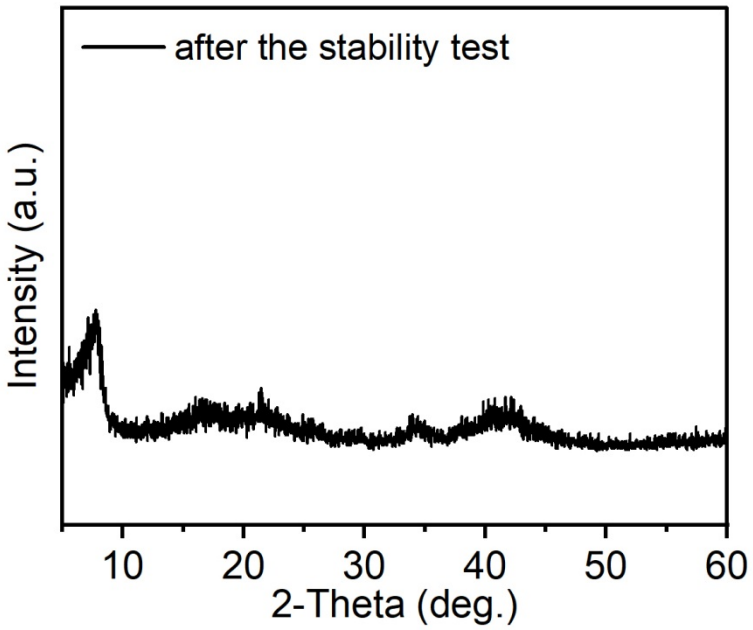

Figure S15. XRD pattern of the post-electrolysis P-$Ti_3C_2T_x$.

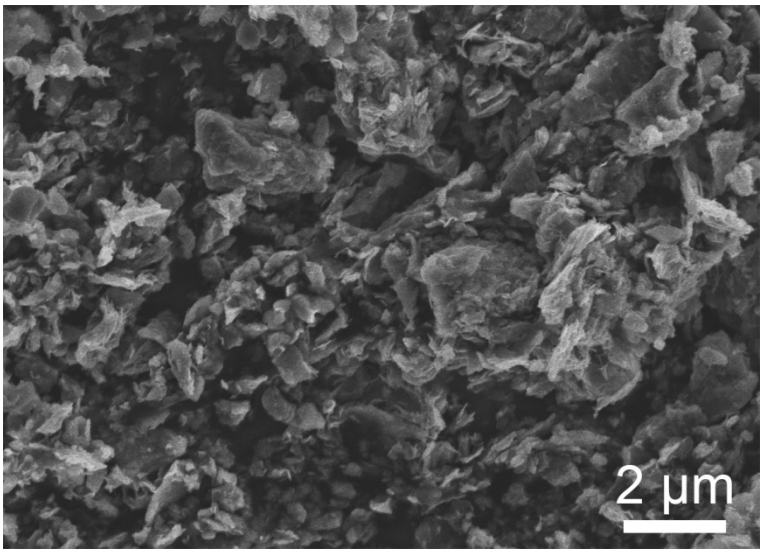

Figure S16. SEM image of the post-electrolysis P-$Ti_3C_2T_x$.

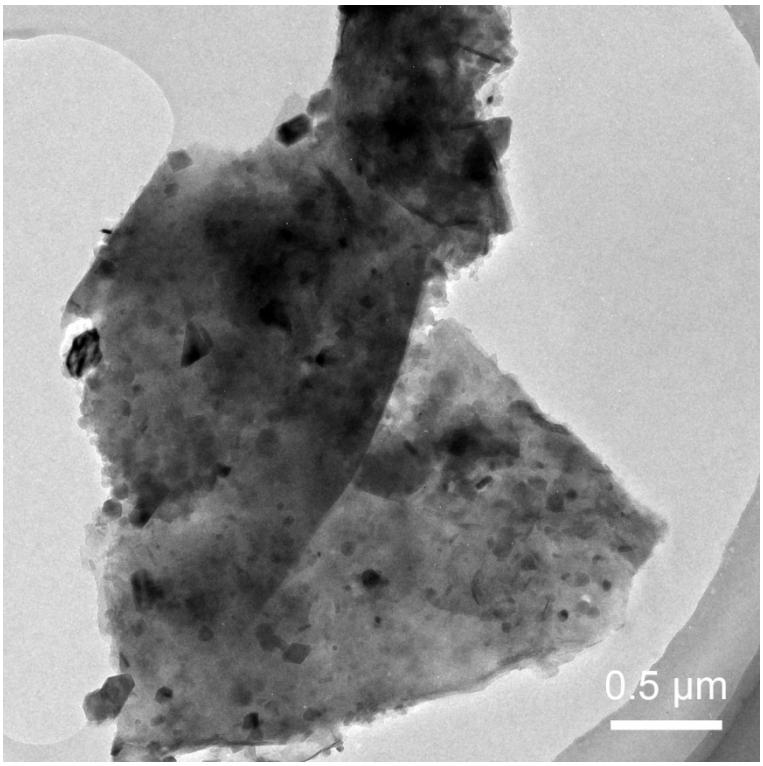

Figure S17. TEM image of the post-electrolysis P-$Ti_3C_2T_x$.

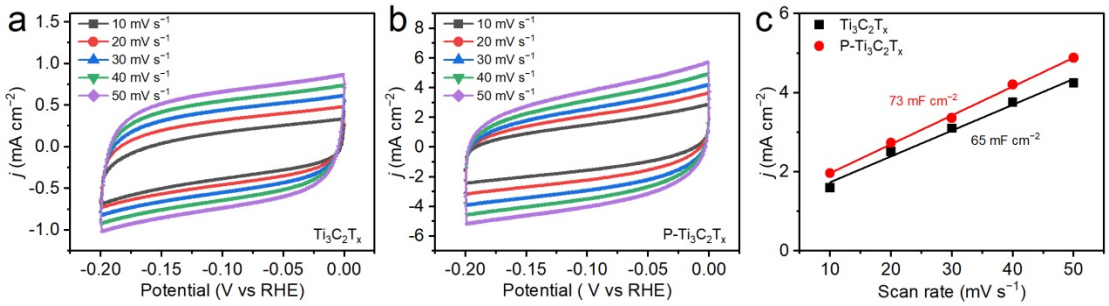

Figure S18. (a) CV curves and (b) C_{dl} measurements of $Ti_3C_2T_x$ and P-$Ti_3C_2T_x$.

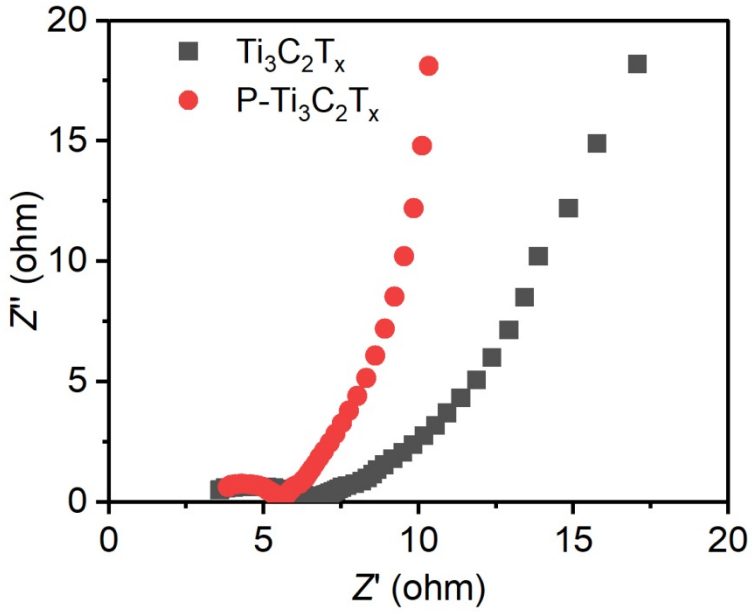

Figure S19. Nyquist plots of $Ti_3C_2T_x$ and P-$Ti_3C_2T_x$.

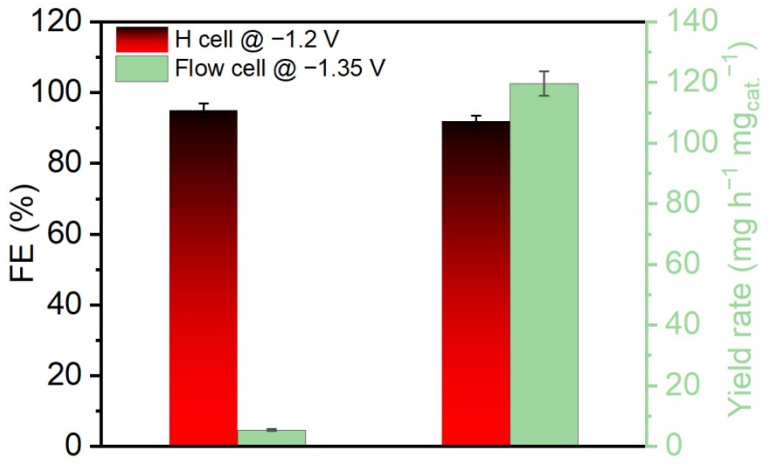

Figure S20. The obtained FE and yield rate at optimal potentials for H cell versus flow cell.

Table S1. Comparisons of the obtained yield rates and FEs in a H-cell.

Catalyst	Electrolyte	Operating potential	NH_3 Production Rate	FE_{NH3}	Ref.
Rh@Cu SA	0.1 M Na_2SO_4 with 0.1 M KNO_3	-0.2 V vs. RHE	1.27 mmol h^{-1} cm^{-2}	93%	Angew. Chem. Int. Ed. 2022, 61: e202202556
Cu-Pd/C nanobelts	0.1 M KOH with 10 mM KNO_3	-0.4 V vs. RHE	220.8 μg mg_{cat}^{-1} h^{-1}	62.3%	ACS Appl. Mater. Interfaces. 2022, 14: 30969
Cu-CuO	0.5 M Na_2SO_4 and 50 mM $NaNO_3$	-0.8 V vs. RHE	3.17 mol h^{-1} g^{-1}	98.7 %.	J Hazard Mater. 2022, 439: 129653
Cu_2O/CuO@C	1.0 M KOH + 50 mM KNO_3	-0.25 V vs. RHE	0.046 mmol h^{-1} cm^{-2}	93.05%	J. Power Sources. 2022, 204: 543
CoP/TiO_2@TP	0.1 M NaOH with 0.1 M $NaNO_3$	-0.5 V / -0.3 V vs. RHE	499.8 μmol h^{-1} cm^{-2}	95.0%	Mater. Today Phys. 2022; 28:100854
Co/CoO NSAs	0.1 M Na_2SO_4	-1.3 V vs. SCE	194.46 μmol h^{-1} cm^{-2}	93.8%	Sci. China Chem. 2020, 63: 1469
FeOOH/CP	0.1 M PBS with 0.1 M $NaNO_3$	-0.5 V / -0.8 V vs. RHE	2,419 μg h^{-1} cm^{-2}	92%	ACS Appl. Mater. Interfaces. 2022, 14: 17312
TiO_{2-x}	0.5 M Na_2SO_4	-1.6 V Vs. SCE	0.045 mmol h^{-1} mg^{-1}	85.0%	ACS Catal. 2020; 10:3533
CoO_x nanosheets	0.1 M KOH	-0.3 V vs. RHE	36.62 mg h^{-1} cm^{-2}	93.4±3.8%	ACS Catal. 2021; 11:15135
Co_3O_4 nanoparticles	0.11 M in 1 M NaOH	-0.7 V vs. RHE	39.60 mg h^{-1} cm^{-2}	96.08%	Adv. Energy Mater. 2022, 12: 2202105
Ag/Cu_2O	0.5 M Na_2SO_4	-0.80 V vs. RHE	0.225 mmol h^{-1} cm^{-2}	96.45%	J. Catal. 2022; 406:39
PdCoO/NF	0.5 M K_2SO_4 with 200 mg L^{-1} of NO_3^--N	-1.3 V vs. SCE	0.2044 mmol h^{-1} cm^{-2}	88.6%	ACS Appl. Mater. Interfaces. 2022, 14: 13169
Rh_xS_y/C	0.1 M HNO_3	0.1 V vs. RHE		67%	Catal. Sci. Technol. 2021; 11:7331

Fe–SnS_2/CC	0.1 M $NaNO_3$	-0.8 V / -0.7 V vs. RHE	7.2 mg h_{-1} cm_{-2}	85.6%	Dalton Trans. 2022, 51: 10343
Cu-SnS_{2-x}	0.1M KNO_3	-0.7 V vs. RHE	0.63 mmol h^{-1} mg_{cat}^{-1}	93.8%	J. Mater. Chem. A, 2023, 11: 2014
NCS-2	1 M KOH	-0.4 V vs. RHE	2,388.4 μg h^{-1} cm^{-2}	85.3%	Appl. Catal., B. 2023, 324: 122193
Fe SACs	0.1M K_2SO_4 and 0.5 M KNO_3	−0.66 V vs. RHE	0.46 mmol h^{-1} cm^{-2}	~ 75%	Nat Commun. 2021; 12:2870
P-$Ti_3C_2T_x$	0.5 M K_2SO_4 + 0.1 M KNO_3	-1.2 V vs RHE	5.39 mg h^{-1} mg_{ca1}^{-1}	95%	This work

Table S2. Comparisons of the obtained yield rates and FEs in a flow-cell.

Catalyst	Electrolyte	Current density (mA cm^{-2})	NH_3 Production Rate	FE_{NH3}	Ref.
Bi-FeS_2	1 M KOH with 0.1 M NO_3^-	1023.2 @ -0.7 V vs. RHE	83.7 mg h^{-1} cm^{-2}	99.2% (-0.7 V vs RHE)	ACS Nano 2023, 17: 21328
Cu/MnOOH	1 M KOH with 0.5 M NO_3^-	700 @ -0.8 V vs. RHE	55.51 mg h^{-1} cm^{-2}	96.8% (-0.8 V vs RHE)	Chinese Chem. Lett. 2024, 10.1016/j.cclet.2024.109958
$Co_{1-x}Cu_x$	1 M KOH with 0.05 M NO_3^-	177@ -0.03 V vs. RHE	NA	95% (-0.03 V vs RHE)	J. Phys. Chem. C 2022, 126: 6982
NiCo LDH/Cu NW	1 M KOH with 0.1 M NO_3^-	570 @ -0.214 V vs. RHE	2.72 mmol h^{-1} cm^{-2}	91.71% (-0.245 V vs RHE)	ACS Catal. 2023, 13: 14670
Cu(x)-OMS-1	0.1 M NaOH with 0.1 M $NaNO_3$	148 @ -1.0 V vs. RHE	0.69 mmol h^{-1} cm^{-2}	99.7% (-1.0 V vs RHE)	Green Chem. 2023, 25: 10549
Fe_2O_3/Fe–N–C	1 M KOH + 0.16 M KNO_3	1265 @ -1.2 V vs. RHE	6 mmol h^{-1} cm^{-2}	90% (-0.4 V vs RHE)	Adv. Mater. 2024, 2401133
Co_3O_4	1 M KOH with 0.3 M NO_3^-	250 @ -0.25 V vs RHE	~1.35 mmol h^{-1} cm^{-2}	85.15% (-0.25 V vs RHE)	Nao Res. 2024, 17: 3902
P-$Ti_3C_2T_x$	1 M K_2SO_4 + 0.5 M KNO_3	1000 @-1.30 V vs RHE	123.5 mg h^{-1} mg_{cal}^{-1}	92%	This work

References

[1] Y. Ren, F. Tian, L. Jin, Y. Wang, J. Yang, S. You and Y. Liu, *Environ. Sci. Technol.* **2023**, 57, 10458.

[2] X. Yang, G. Wei, J. Cao, Z. Ding, R. Yuan, J. Long and C. Xu, *ACS Sustain. Chem. Eng.* **2024**, 12, 3378-3389.